

1 Last century warming over the Canadian Atlantic shelves linked to weak
2 Atlantic Meridional Overturning Circulation

3

4

5 **Authors**

6 B. Thibodeau^{1,2,†*}, C. Not^{1,2,†}, J. Zhu³, A. Schmittner⁴, D. Noone⁴, C. Tabor⁵, J. Zhang⁶, Z. Liu⁷

7

8 **Affiliations**

9 ¹Department of Earth Sciences, The University of Hong Kong, Hong Kong SAR

10 ²The Swire Institute of Marine Science, The University of Hong Kong, Hong Kong SAR

11 ³Department of Earth and Environmental Sciences, University of Michigan, United-States of
12 America

13 ⁴College of Earth, Ocean, and Atmospheric Sciences, Oregon State University, United-States
14 of America

15 ⁵Center for Integrative Geosciences, University of Connecticut, United-States of America

16 ⁶CCS-2 and CNLS, Los Alamos National Laboratory, Los Alamos, New Mexico, United-
17 States of America

18 ⁷Atmospheric Science Program, Department of Geography, The Ohio State University, United-
19 States of America

20

21 *Correspondence to: bthib@hku.hk

22 † Equal contribution

23

24

25 **Abstract**

26 The Atlantic meridional overturning circulation (AMOC) is a key component of the global
27 climate system. Many models predict a weakening or even a collapse of the AMOC under
28 future climate change. Recent studies suggested a 20th century weakening of the AMOC of
29 unprecedented amplitude (~ 15%) over the last millennium. Here, we present a record of $\delta^{18}\text{O}$
30 in benthic foraminifera from sediment cores retrieved from the Laurentian Channel and
31 demonstrate that the $\delta^{18}\text{O}$ trend is linked to the strength of the AMOC. In this 100-year record,
32 the AMOC signal decreased steadily to reach its minimum value in the late 1970's, where the
33 weakest AMOC signal then remains constant until 2000. We present a longer $\delta^{18}\text{O}$ record of
34 1,500 years and highlight the uniqueness of these high $\delta^{18}\text{O}$ values over that period. Moreover,
35 the long record is also characterized by statistically heavier $\delta^{18}\text{O}$ during the Little Ice age,
36 suggesting a relatively weak AMOC.

37

38

39 **1. Introduction**

40 The Atlantic meridional overturning circulation (AMOC) encompasses the advection
41 of warm and saline waters in the upper ocean to the northern parts of the Atlantic, where it
42 cools, becomes denser and sinks, ultimately creating North Atlantic deep water. Both
43 observational and modeling studies have suggested that the strength of this oceanic circulation
44 cell is not constant through time (Bohm et al., 2015; Rahmstorf et al., 2015), and that these
45 changes drive many other climatic events across wide ranges of spatial and temporal scales
46 (Delworth et al., 2008). Weakening of the AMOC as a response to warming and/or high latitude
47 freshwater release is a common feature of many climate models (Bakker et al., 2016; Jungclaus
48 et al., 2006; Krebs & Timmermann, 2007; Stouffer et al., 2006; Yang et al., 2016; Yu et al.,
49 2016). However, a recent study suggested that current models are not sensitive enough in their
50 AMOC response (Liu et al., 2017), which implies that previous model projections of collapse
51 probabilities are underestimated. The possibility of an AMOC collapse under global warming
52 is a major concern due to its potentially dramatic impacts on oceanic circulation and global
53 climate. The consequences of freshwater input near sites of deep water formation are a
54 contemporary concern as the total freshwater storage of the North Atlantic increased by 19 000
55 km³ between 1961 and 1995 (~0.02 Sv on average; Curry, 2005). This freshwater is transported
56 to the Labrador Sea and creates salinity anomalies (Luo et al., 2016). It is therefore increasingly
57 critical that we understand the impacts of climate change and freshwater release on convection
58 in the Labrador Sea and its corresponding impact on AMOC intensity (Gregory et al., 2005).
59 This is especially true if we are to identify the forcing(s) responsible for the ongoing AMOC
60 weakening (Bakker et al., 2016; Thornalley et al., 2018).

61 High-resolution modeling (~10 km ocean, ~50 km atmosphere) suggests a robust
62 relationship between a weakening AMOC and the decrease in the proportion of Labrador-
63 derived water (Labrador Subarctic Slope Water : LSSW) entering the Northwest Atlantic shelf
64 compared to Atlantic-derived water (Atlantic Temperate Slope Water : ATSW) under climate
65 change (Saba et al., 2016; Fig 1a). Interestingly, historical instrumental temperature data
66 suggest a significant reorganisation of the Northwest Atlantic slope currents from the bottom
67 water of the St. Lawrence Estuary (Gilbert et al., 2005). The significant bottom water warming
68 (+1.7°C) during the twentieth-century was attributed to a decrease in the proportion (72 to
69 53%) of cool LSSW entering the Laurentian Channel (Gilbert et al., 2005). This warming was
70 suggested to be unique over the last millennium (Thibodeau et al., 2010a) and the last ~6,000
71 years (Thibodeau et al., 2013). This major change in the regional oceanography has severe

72 environmental consequence, as the ATSW is characterized by lower dissolved oxygen content
73 than the LSSW which, in conjunction with localized eutrophication, is thought to be
74 responsible for the development of the permanent hypoxic zone in the St. Lawrence Estuary
75 (Benoit et al., 2006; Gilbert et al., 2005; Lefort et al., 2012; Thibodeau et al., 2006; Thibodeau
76 et al., 2010b). As detailed in figure 1, the recirculation gyre is considered to be controlled by
77 the strength of the formation of deep water in the Labrador Sea and thus by the strength of the
78 deep western boundary current (DWBC) (Zhang et al., 2007). A strong recirculation gyre keeps
79 the Gulf Stream path well separated from the coast (Fig 1a) and allows for southern penetration
80 of the LSSW. In episodes of weak convection characteristic of modern conditions (Rahmstorf
81 et al., 2015), a larger proportion of the warm water from the Gulf Stream and ATSW is
82 expected to be found in the Laurentian Channel bottom water (Fig 1b). It was further suggested
83 that the westward transport of Labrador current water along the continental shelf edge to the
84 south of the Grand Banks of Newfoundland is the most important factor driving temperature
85 and salinity variability in the Laurentian Channel (Petrie & Drinkwater, 1993; Fig 1c). Thus,
86 the observed warming in the Laurentian Channel and the western North Atlantic could be
87 linked to the weakened state of the AMOC (Caesar et al., 2018; Rahmstorf et al., 2015;
88 Thornalley et al., 2018).

89 Here, we present two high-resolution records of oxygen isotope ($\delta^{18}\text{O}$) measurements
90 of the benthic foraminiferan *Globobulimina auriculata* covering the last century and the last
91 1,500 years respectively. We demonstrate how these records can be used to track sub-surface
92 temperature of the western North Atlantic. We then tested this paleotemperature record against
93 instrumental measurements, new model simulations, AMOC index and other AMOC-related
94 proxies to link our record to the AMOC intensity. As such, we provide here a new
95 paleoreconstruction of the AMOC intensity and highlight that the AMOC is probably at its
96 weakest state since the last 1,500 years. While the uncertainties are larger when we investigate
97 older periods, we further report statistically heavier $\delta^{18}\text{O}$ during the Little Ice Age (LIA), which
98 could be related to weaker AMOC conditions during that time. Thus, our record is significant
99 for the investigation of the potential mechanisms responsible for the last century AMOC
100 weakening.

101

102 2. Methods

103 We investigated the effects of an AMOC reduction on the western North Atlantic slope
104 water temperature via freshwater perturbation experiments using two climate models: the
105 University of Victoria climate model (UVic v2.9) and the water isotope-enabled Community
106 Earth System Model (iCESM1.3). The UVic model is a climate model of intermediate
107 complexity including an ocean general circulation model at coarse resolution ($3.6 \times 1.8^\circ$, 19
108 vertical levels), a single-layer atmospheric energy-moisture balance model, a dynamic-
109 thermodynamic sea ice model, and biogeochemical components. The freshwater perturbation
110 experiment analyzed here has 0.05 Sv freshwater discharged into the North Atlantic between
111 $45\text{--}65^\circ\text{N}$ and $60\text{--}0^\circ\text{W}$ for 100 years. Readers are referred to previous publications for a detailed
112 description of the experimental setup (Schmittner & Lund, 2015).

113 The water isotope-enabled Community Earth System Model version 1.3 (iCESM) is a
114 state-of-the-art fully coupled Earth system model with the capability to simulate the oxygen
115 isotopes in the hydrological cycle (Nusbaumer et al., 2017; Wong et al., 2017; Zhang et al.,
116 2017; Zhu et al., 2017a). The numerical experiments analyzed here are from a recent study
117 (Zhu et al., 2017b). The simulations were conducted with a horizontal resolution of $1.9 \times 2.5^\circ$
118 (latitude \times longitude) for the atmosphere and land, and a nominal 1° for the ocean and sea ice.
119 The ocean model consists of 60 uneven levels with an interval of ~ 10 m for the upper 200 m.
120 The preindustrial control simulation was run for 500 years, with forcing fixed at the values
121 from 1850 A.D., and water isotopes in the ocean initialized from the Goddard Institute for
122 Space Studies interpolated observational dataset (LeGrande & Schmidt, 2006). In the
123 freshwater perturbation experiment, 0.10 Sv of isotopically depleted fresh water was
124 discharged into the northern North Atlantic ($50\text{--}70^\circ\text{N}$) for 100 years. The $\delta^{18}\text{O}$ signature of the
125 freshwater forcing was set as -30 ‰ SMOW (Hillaire-Marcel & Causse, 1989). The simulation
126 of $\delta^{18}\text{O}$ in the model helps to test our interpretation of the benthic $\delta^{18}\text{O}$ records in the Laurentian
127 channel. The response of carbonate $\delta^{18}\text{O}$ (‰ PDB) to freshwater forcing is calculated in the
128 model with the simulated ocean temperature and $\delta^{18}\text{O}$ (‰ SMOW) of seawater, using the
129 paleotemperature equation of Shackleton (1974).

130 We then compiled $\delta^{18}\text{O}$ data (‰ VPDB) measured on the benthic foraminifera
131 *Globobulimina auriculata* in two sediment cores (CR02-23 and MD99-2220; core details in
132 S1-2) from the Laurentian Channel (Fig 1a). The calcareous shells were picked under binocular
133 and roasted at ~ 200 °C for about 2 hours in order to eliminate organic matter. Samples were
134 analyzed with a Micromass Isoprime™ isotope ratio mass spectrometer in dual inlet mode
135 coupled to a MultiCarb™ preparation system. The CO_2 was extracted at 90°C by acidification

136 with concentrated H₃PO₄. The analytical reproducibility determined by replicate measurements
137 of internal standard carbonate material was routinely better than 0.05 ‰, which is equivalent
138 to a precision of about 0.15-0.20°C in temperature.

139

140 **3. Results and Discussion**

141 *3.1. Modelled effect of reduced AMOC on subsurface temperature*

142 To test the link between AMOC strength and subsurface warming, the AMOC strength
143 was reduced in two models (iCESM and UVic) (see detailed results in S3). Both models used
144 here produced a large-scale subsurface warming in the northwest Atlantic at 45°N (Fig S1)
145 with a maximum of 1–3°C around 50°W. The AMOC reduction obtained with the UVic model
146 (~ 17 %) is consistent with the most recent estimate of weakening (Caesar et al., 2018;
147 Rahmstorf et al., 2015; Thornalley et al., 2018). This subsurface warming of the western North
148 Atlantic under weak AMOC conditions is expected from field data (Dima & Lohmann, 2010),
149 theory (Petrie & Drinkwater, 1993; Zhang, 2008; Zhang et al., 2007), coarse (this study) as
150 well as high-resolution and eddy-permitting models (Brickman et al., 2018; Caesar et al., 2018;
151 Saba et al., 2016; Thornalley et al., 2018). Thus, the warming can be considered a robust
152 fingerprint of the weakened AMOC.

153

154 *3.2. Influence of temperature and water mass contribution on the δ¹⁸O record*

155 The isotopic signature of oxygen in *Globobulimina auriculata* tests is a good proxy of
156 temperature change in the Laurentian Channel during the last century (Thibodeau, et al.,
157 2010a). The warming instrumentally observed in the Laurentian Channel bottom water seems
158 well captured by *Globobulimina auriculata* δ¹⁸O in the high sedimentation box-core CR02-23
159 samples (Fig 2), as the δ¹⁸O decreases from 1940 to 2000 by about 0.4 ‰ synchronously with
160 the 2°C increase in temperature from the bottom water of the St. Lawrence Estuary. However,
161 the δ¹⁸O of benthic foraminifera also records the change in the proportion of water masses
162 entering the Laurentian channel, as these water masses are characterized by different isotopic
163 conditions. Using the isotopic signature of both water mass (ATSW = 0.5 ‰ and LSSW = -0.5
164 ‰), it was estimated that the proportion of these water masses is currently about 50-50%
165 (Thibodeau et al., 2010a). Based on dissolved oxygen and temperature, it was hypothesized
166 that the proportion of ATSW entering the Laurentian channel was much lower in 1940 at about
167 30% (Gilbert et al., 2005), which imply an increase of δ¹⁸O by about 0.2 ‰ between 1940 and

168 2000. We observed that the $\delta^{18}\text{O}$ of seawater exhibits an enrichment of 0.2 to 0.3 ‰ in the
169 subsurface western North Atlantic in the freshwater perturbation experiment using iCESM (Fig
170 S3), which is coherent with the magnitude of the increase in the proportion of ATSW entering
171 the Laurentian Channel inferred from temperature and dissolved oxygen changes (Gilbert et
172 al., 2005; Thibodeau et al., 2010a)). Considering a relationship of about $-0.3 \text{ ‰}/^\circ\text{C}$, one would
173 expect a decrease of -0.6 ‰ in the $\delta^{18}\text{O}$ of *Globobulimina auriculata* considering the
174 instrumentally-measured 2°C warming in the bottom water between 1940 and 2000. However,
175 we only observed a depletion of about 0.4 ‰ , which is coherent with the modelled enrichment
176 due to the change in water masses. We therefore suggest that the Laurentian Channel benthic
177 $\delta^{18}\text{O}$ record is strongly influenced by AMOC intensity via the advection of the western North
178 Atlantic subsurface temperature and water mass dynamics.

179

180 3.3. Comparison with other AMOC-related proxies over the last century

181 An annually-resolved $\delta^{15}\text{N}$ record retrieved from soft corals over the Canadian shelf
182 shows a high degree of similarity with both the $\delta^{18}\text{O}$ record and the instrumental record of
183 temperature (Fig 2). This record was interpreted as an increase in the proportion of ATSW
184 reaching the Canadian shelf, a unique event of the last 1800 years (Sherwood et al., 2011) and
185 is consistent with the AMOC index (Caesar et al., 2018; Rahmstorf et al., 2015). The CR02-23
186 $\delta^{18}\text{O}$ record presented here is also in agreement with the AMOC index over the 1940-2000
187 period despite some leads and lags that can be attributed to either the different resolution and
188 time integration of the respective proxies. The leads and lags could also be caused by the fact
189 that the AMOC-index and our record integrate different signals; the AMOC-index estimates
190 the difference in the temperature anomalies between the sub-polar gyre and the Northern
191 hemisphere while the $\delta^{18}\text{O}$ captures the temperature and water mass distribution of the slope
192 water. Despite the potential caveats, the similarity between our $\delta^{18}\text{O}$ record, the temperature-
193 based AMOC index, and instrumental data adds to the evidence linking the strength of the
194 AMOC with the western North Atlantic subsurface temperature (Marcott et al., 2011; Petrie &
195 Drinkwater, 1993; Saba et al., 2016), which implies that temperature can be used to diagnose
196 the state of AMOC, as done previously (Caesar et al., 2018; Rahmstorf et al., 2015; Thornalley
197 et al., 2018; Zhang, 2008). The $\delta^{18}\text{O}$ of benthic foraminifera in the Laurentian Channel can
198 thus provide crucial information to reconstruct AMOC variability during the last century
199 despite the fact that it incorporates both the temperature and the water mass signal.

200 The trend of $\delta^{18}\text{O}$ derived from the benthic foraminifera in long piston core MD99-
201 2220 (hereafter MD) during the 20th century is unique in its magnitude for the last 1,500 years.
202 While the current global warming trend could be invoked to explain this warming, we stress
203 that neither of the parent water masses warmed significantly during the same period (Gilbert
204 et al., 2005). Moreover, the absolute value of 1.5-2.0°C is much larger than the ~0.4°C
205 attributed to the global trend (IPCC, 2013). Potential control from the North Atlantic
206 Oscillation can also be discarded as no correlation with the temperature time series was
207 observed (Gilbert et al., 2005). While still controversial, the reduction of the AMOC since the
208 late 1930s and the drastic shift in North Atlantic overturning cell at the beginning of the 70's
209 was already identified using field data (Dima & Lohmann, 2010). The agreement between the
210 instrumental data, various climate archives, the two models, and the AMOC index lead us to
211 conclude that the weakening of the AMOC is a major factor causing the sub-surface warming
212 recorded in the sediment cores and corals compiled here. The evidence presented here thus
213 reinforces previous findings and provides complementary geological evidence for the 20th
214 century AMOC slowdown.

215 While our record and modeling results strengthens the previous hypothesis regarding the
216 recent weakening of the AMOC and its consequences in the western North Atlantic, it also
217 highlights some discrepancies such as the 100-year difference in the beginning of the
218 weakening of the convection in the Labrador Sea (Thornalley et al., 2018) and the AMOC
219 (Caesar et al., 2018; Rahmstorf et al., 2015). Interestingly, our $\delta^{18}\text{O}$ record, interpreted as
220 being controlled by DWBC strength, mimics the AMOC index with a weakening starting
221 within the last century as opposed to the 19th century decline in the Labrador Sea convection
222 (Thornalley et al., 2018). While it is conceivable to invoke a potential lag between a reduced
223 convection in the Labrador Sea and its expression on surface waters, the pre-AD 1200
224 paleorecord does not seem to exhibit such lag, as the $\delta^{18}\text{O}$ matches the proxy for convection in
225 the Labrador Sea (Fig 3; see section 3.5). However, the amplitude of the recent weakening is
226 unique over this period and so caution should be exercised when directly using the paleorecord
227 to find the cause of this apparent mismatch. Moreover, the potential absence of decline in
228 Labrador Sea convection during the last part of 20th century (Böning et al., 2016) and the last
229 couple of decades (Yashayaev & Loder, 2016) also highlight the need to reconcile estimation
230 of convection in the Labrador Sea and the integrative AMOC proxies.

231 While it is possible to use our $\delta^{18}\text{O}$ proxy in longer reconstruction, it is not possible to
232 constrain $\delta^{18}\text{O}$ change solely to a change in the proportion of water masses as we did for the

233 last century since it is not known if the parent water masses temperature varied. As such,
234 potential temperature changes of the Gulf Stream (and ATSW) and Labrador Current (and
235 LSSW) should also be considered as a potential driver of $\delta^{18}\text{O}$ when analysing the pre-20th
236 century record.

237

238 *3.4. The 1600-1900 period*

239 While we observe a step-wise decrease in the AMOC starting in the late 15th century,
240 these variations are within the natural range of variability of our $\delta^{18}\text{O}$ record (Fig S6). However,
241 the 1600-1899 $\delta^{18}\text{O}$ values in core MD are significantly heavier compared to the pre-1600
242 record, suggesting a statistically weaker AMOC during the LIA. Alternative explanations for
243 the low $\delta^{18}\text{O}$ during this period include a warming of either parent water mass, which would
244 be counterintuitive for this time period (Keigwin, 1996). While the $\delta^{18}\text{O}$ of the Gulf Stream
245 increased by about 0.1 ‰ between 1600 and 1900 (Saenger et al., 2011), it would account only
246 for half of the increase observed in the MD core. Thus, a change in the proportion of the water
247 masses entering the Laurentian Channel due to a weaker AMOC cannot be excluded at this
248 point. At about AD 1850-1875, the sharp depletion in $\delta^{18}\text{O}$ is synchronous with the sudden
249 decrease in DWBC intensity and Labrador Sea convection, which might be due to the
250 beginning of the post-LIA ice cap melt and the consequent freshening of the Labrador Sea
251 surface water (Koerner, 1977; Koerner & Fisher, 1990). While the MD core might record a
252 weakened AMOC state during most of the LIA (1625-1850), its step-wise nature, rather than a
253 continual weakening trend observed in the sortable silt record, suggests that the signal reflects
254 DWBC intensity (Fig 3c). This highlights a potential discrepancy between how the AMOC
255 signal is expressed in the $\delta^{18}\text{O}$ record and how it is translated in current velocity at 2,000 m
256 depth, where the 48JPC and 56JPC cores were retrieved (Thornalley et al., 2018). Here, the
257 potential interference from temperature and salinity changes in the parent water masses should
258 be investigated in greater detail.

259

260 *3.5. The pre-1600 period*

261 The comparison of the MD core with the AMOC index highlights the absence of any
262 trend within these two records throughout this period (Fig 3a). However, the MD record is
263 characterized by more variability pre-AD 1500. This may be caused by the construction of the
264 AMOC index based on multiple different proxies of SST in both the western North Atlantic

265 and the subpolar North Atlantic, whereas the MD core records the subsurface signal at a single
266 location, implying that the AMOC index integrates a much larger oceanic area and reduces the
267 variability (Rahmstorf et al., 2015). This might alternatively be explained by subsurface
268 temperature being slightly more sensitive to convection relative to the surface temperature.
269 This is supported by the agreement pre-AD 1500 between the MD core and temperature and
270 salinity reconstructions from the Labrador Sea (Fig 3b), which are considered effective proxies
271 for Labrador Sea convection (Moffa-Sánchez et al., 2014). Thus, the $\delta^{18}\text{O}$ seems to record most
272 of the natural variability of the Labrador Sea convection over that period.

273

274 **4. Implications**

275 Our record adds to the existing paleoreconstructions of AMOC for the last millennium and
276 highlights the statistically weaker state of the AMOC during the 20th century. The data provided
277 here are important to disentangle the potential causes of the 20th century weakening, as they
278 record sub-surface processes, which is different from the previously-published surface AMOC
279 index (Rahmstorf et al., 2015) and reconstruction of the DWBC (Thornalley et al., 2018).
280 Moreover, the heavy $\delta^{18}\text{O}$ recorded during the LIA suggests a potential weakening of the
281 AMOC during that period. These data could be used with temperature reconstructions of the
282 Labrador current and Gulf Stream in order to further constrain the implication of the heavy
283 $\delta^{18}\text{O}$ values in the Laurentian Channel. Our $\delta^{18}\text{O}$ record thus captures crucial information that
284 will contribute to a better understanding of AMOC variability throughout the last 1,500 years
285 and its drivers.

286

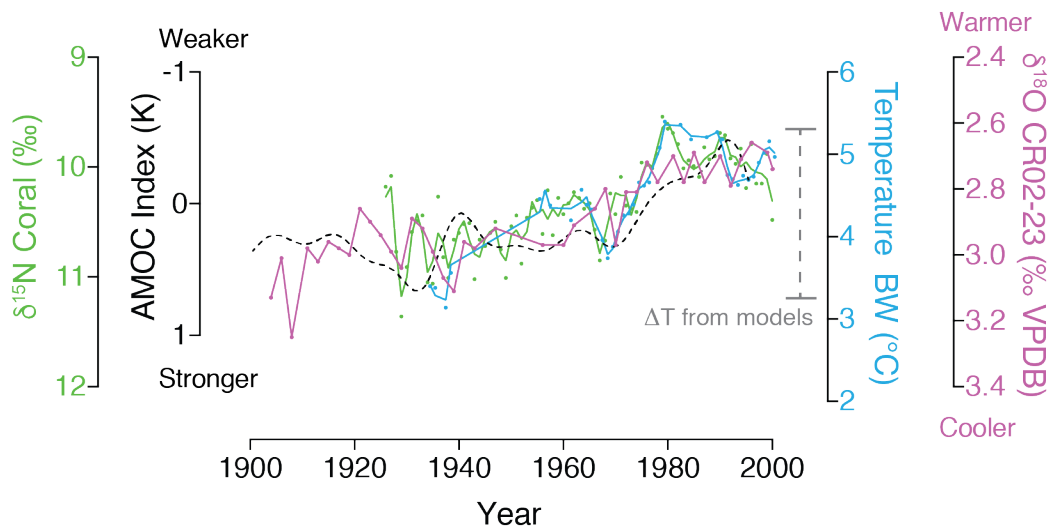
287 **5. Acknowledgments**

288 **Author contributions:** BT and CN designed the study, BT performed isotopic analyses
289 on CR02-23 and MD99-2220, AS performed the modeling with UVic2.9 and JZhu
290 performed the modeling with iCESM1.3. BT and CN wrote the manuscript with the
291 contribution of JZhu, AS, DN, CT, JZhang and ZL.
292

293 **Data and materials availability:** All data used in this paper are available in the online
294 material. The iCESM model codes are available through the National Center for
295 Atmospheric Research software development repository. Data for the iCESM model
296 are available by reasonable request to JZ (jjazhu@umich.edu). The UVic model cores
297 are available at <http://climate.uvic.ca/model/>. Data for the UVic experiment are
298 available at <http://www.clim-past.net/11/135/2015/cp-11-135-2015-supplement.zip> or
299 by reasonable request to AS (aschmitt@coas.oregonstate.edu).

313 strength of the northern recirculation gyre (white arrows) (Hogg et al., 1986). The width of the
314 arrows represents the relative strength of the current. White dots indicate the position of core
315 MD99-2220 and CR02-23, which were cored close to each other (respectively at; 48°38.32'N,
316 68°37.93'W; 320m and 48°42.01'N, 68°38.89'W; 345m). The position of corals raised from
317 the Northeast Channel where a $\delta^{15}\text{N}$ time series was recorded is also marked (42°00'N,
318 65°36'W, between 275 and 450 m) (Sherwood et al., 2011). The temperature profile depicts
319 the annually averaged position of the slope waters and how they fill the bottom of the
320 Laurentian Channel.

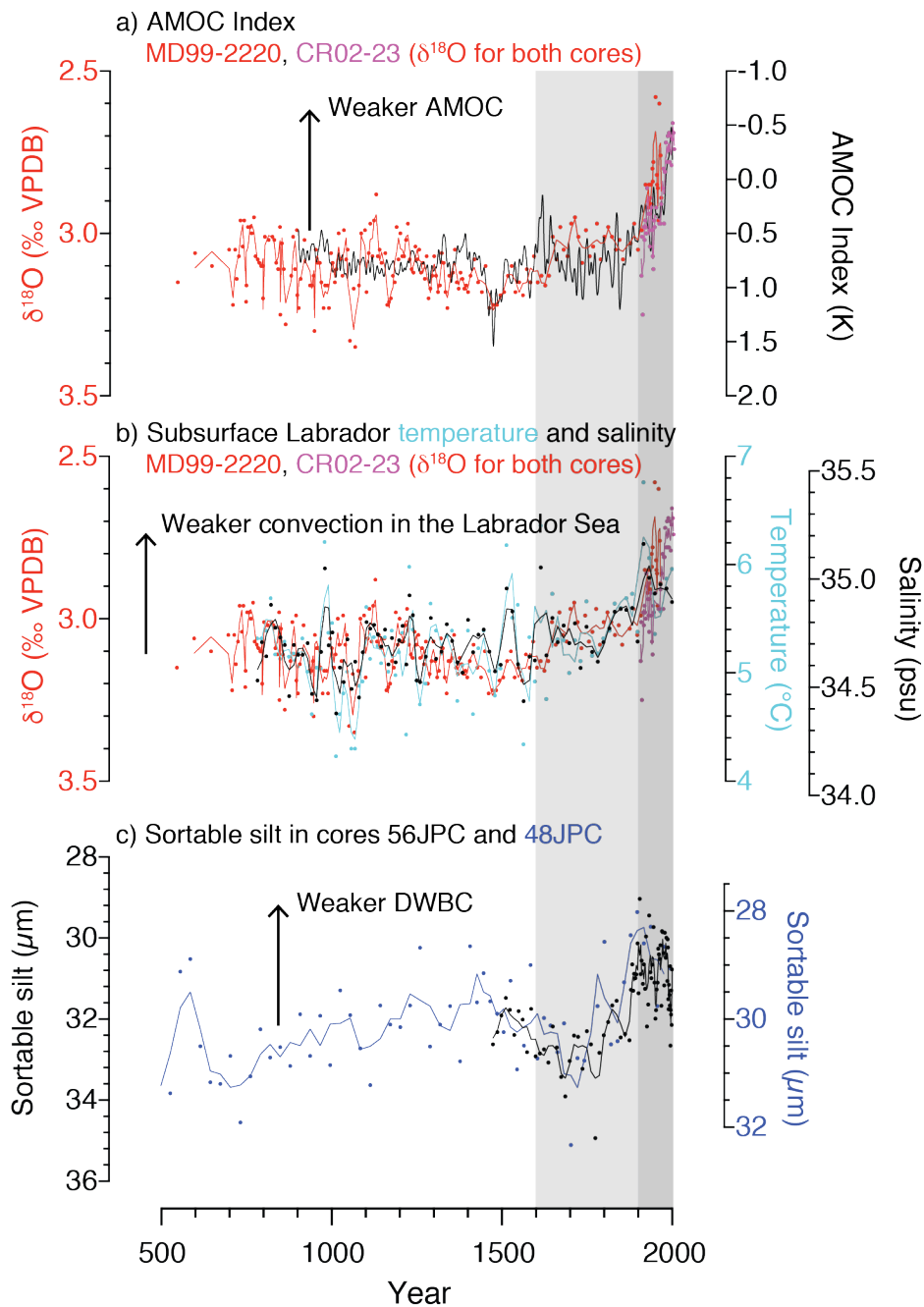
321



323

324 **Figure 2. Proxy validation using instrumental data and paleorecords.** The AMOC
 325 index (Rahmstorf et al., 2015) (black dashed line) and instrumental temperature record of
 326 Laurentian Channel bottom water (Gilbert et al., 2005) (light blue dots and smoothed line; 2nd
 327 order, 2 neighbors) are plotted for the 1900-2000 period along the annually resolved coral $\delta^{15}\text{N}$
 328 record (Sherwood et al., 2011) (green dots and smoothed line; 2nd order, 2 neighbors) that
 329 serves as a proxy of the strength of the northern recirculation gyre and the modal state of the
 330 western North Atlantic circulation. The $\delta^{18}\text{O}$ of benthic foraminifera from core CR02-23
 331 (Thibodeau et al., 2010a) (pink) also shows the same general pattern during that period. The
 332 average temperature increase (2°C) obtained at 400 m deep in the western North Atlantic in
 333 our modelled AMOC-weakening experiments is indicated by the gray bracket.

334



336

337

Figure 3. Comparison of North Atlantic climate archives covering the last millennium. The first panel **a)** comparison of composite (MD99-2220; red and CR02-23; pink) $\delta^{18}\text{O}$ *Globobulimina auriculata* record (smoothed lines; 2nd order, 2 neighbors) with the AMOC index (Rahmstorf et al., 2015) (black line). **b)** similarity of the composite (MD99-2220; red and CR02-23; pink) $\delta^{18}\text{O}$ record (smoothed lines; 2nd order, 2 neighbors) with reconstructed subsurface temperature (light blue dots) and salinity (black dots) of the Labrador Sea (Moffa-Sánchez et al., 2014), which are indicative of convection in the Labrador Sea (smoothed lines;

343

344 2nd order, 2 neighbors). **c)** sortable silt from two sediment cores retrieved off Cape Hatteras, a
345 proxy of the deep western boundary current (smoothed lines; 2nd order, 2 neighbors)
346 (Thornalley et al., 2018). Grey bars highlight the LIA and the 20th century.

347

348

349 Bakker, P., Schmittner, A., Lenaerts, J. T. M., Abe-Ouchi, A., Bi, D., van den Broeke, M. R.,
350 et al. (2016). Fate of the Atlantic Meridional Overturning Circulation: Strong decline
351 under continued warming and Greenland melting. *Geophysical Research Letters*,
352 *43*(23), 12,252–12,260. <https://doi.org/10.1002/2016GL070457>

353 Benoit, P., Gratton, Y., & Mucci, A. (2006). Modeling of dissolved oxygen levels in the
354 bottom waters of the Lower St. Lawrence Estuary: Coupling of benthic and pelagic
355 processes. *Marine Chemistry*, *102*(1–2), 13–32.
356 <https://doi.org/10.1016/j.marchem.2005.09.015>

357 Bohm, E., Lippold, J., Gutjahr, M., Frank, M., Blaser, P., Antz, B., et al. (2015). Strong and
358 deep Atlantic meridional overturning circulation during the last glacial cycle. *Nature*,
359 *517*(7532), 73–76. Retrieved from <http://dx.doi.org/10.1038/nature14059>

360 Böning, C. W., Behrens, E., Biastoch, A., Getzlaff, K., & Bamber, J. L. (2016). Emerging
361 impact of Greenland meltwater on deepwater formation in the North Atlantic Ocean.
362 *Nature Geosci*, *9*(7), 523–527. Retrieved from <http://dx.doi.org/10.1038/ngeo2740>

363 Brickman, D., Hebert, D., & Wang, Z. (2018). Mechanism for the recent ocean warming
364 events on the Scotian Shelf of eastern Canada. *Continental Shelf Research*, *156*, 11–22.
365 <https://doi.org/10.1016/j.csr.2018.01.001>

366 Caesar, L., Rahmstorf, S., Robinson, A., Feulner, G., & Saba, V. (2018). Observed
367 fingerprint of a weakening Atlantic Ocean overturning circulation. *Nature*, *556*(7700),
368 191–196. <https://doi.org/10.1038/s41586-018-0006-5>

369 Curry, R. (2005). Dilution of the Northern North Atlantic Ocean in Recent Decades. *Science*,
370 *308*(5729), 1772–1774. <https://doi.org/10.1126/science.1109477>

371 Delworth, T. L., Clark, P. U., Holland, M., Johns, W. E., Kuhlbrodt, T., Lynch-Stieglitz, J., et
372 al. (2008). The Potential for Abrupt Change in the Atlantic Meridional Overturning
373 Circulation. *Abrupt Climate Change*, 117–162. Retrieved from
374 <http://citeseerx.ist.psu.edu/viewdoc/download?doi=10.1.1.184.709&rep=rep1&type=pdf>
375 <http://downloads.climate.gov/sap/sap3-4/sap3-4-final-report-ch4.pdf>

376 Dima, M., & Lohmann, G. (2010). Evidence for Two Distinct Modes of Large-Scale Ocean
377 Circulation Changes over the Last Century. *Journal of Climate*, *23*(1), 5–16.
378 <https://doi.org/10.1175/2009JCLI2867.1>

379 Ghaleb, B. (2009). Overview of the methods for the measurement and interpretation of short-
380 lived radioisotopes and their limits. *IOP Conference Series: Earth and Environmental*
381 *Science*, *5*, 012007. <https://doi.org/10.1088/1755-1307/5/1/012007>

382 Gilbert, D., Sundby, B., Gobeil, C., Mucci, A., & Tremblay, G. H. (2005). A seventy-two-
383 year record of diminishing deep-water oxygen in the St. Lawrence estuary: The
384 northwest Atlantic connection. *Limnology and Oceanography*, *50*(5), 1654–1666.
385 <https://doi.org/10.4319/lo.2005.50.5.1654>

386 Gregory, J. M., Dixon, K. W., Stouffer, R. J., Weaver, A. J., Driesschaert, E., Eby, M., et al.
387 (2005). A model intercomparison of changes in the Atlantic thermohaline circulation in
388 response to increasing atmospheric CO₂ concentration. *Geophysical Research Letters*,
389 *32*(12), 1–5. <https://doi.org/10.1029/2005GL023209>

390 Hillaire-Marcel, C., & Causse, C. (1989). The late pleistocene Laurentide glacier: Th U
391 dating of its major fluctuations and $\delta^{18}\text{O}$ range of the ice. *Quaternary Research*, *32*(2),
392 125–138. [https://doi.org/10.1016/0033-5894\(89\)90070-7](https://doi.org/10.1016/0033-5894(89)90070-7)

393 Hogg, N. G., Pickart, R. S., Hendry, R. M., & Smethie, W. J. (1986). The northern
394 recirculation gyre of the gulf Stream. *Deep Sea Research Part A, Oceanographic*
395 *Research Papers*, *33*(9), 1139–1165. [https://doi.org/10.1016/0198-0149\(86\)90017-8](https://doi.org/10.1016/0198-0149(86)90017-8)

396 IPCC. (2013). *Climate Change 2013: The Physical Science Basis. Summary for*
397 *Policymakers*. IPCC. Retrieved from
398 <http://medcontent.metapress.com/index/A65RM03P4874243N.pdf>

399 Jungclaus, J. H., Haak, H., Esch, M., Roeckner, E., & Marotzke, J. (2006). Will Greenland
400 melting halt the thermohaline circulation? *Geophysical Research Letters*, 33(17).
401 <https://doi.org/10.1029/2006GL026815>

402 Keigwin, L. D. (1996). The Little Ice Age and Medieval Warm Period in the Sargasso Sea.
403 *Science*, 274(5292), 1503–1508. <https://doi.org/10.1126/science.274.5292.1503>

404 Koerner, R. M. (1977). Devon Island Ice Cap: Core Stratigraphy and Paleoclimate. *Science*,
405 196(4285), 15–18. <https://doi.org/10.1126/science.196.4285.15>

406 Koerner, R. M., & Fisher, D. A. (1990). A record of Holocene summer climate from a
407 Canadian high-Arctic ice core. *Nature*, 343(6259), 630–631.
408 <https://doi.org/10.1038/343630a0>

409 Krebs, U., & Timmermann, A. (2007). Fast advective recovery of the Atlantic meridional
410 overturning circulation after a Heinrich event. *Paleoceanography*, 22(1), 1–9.
411 <https://doi.org/10.1029/2005PA001259>

412 Lefort, S., Gratton, Y., Mucci, a., Dadou, I., & Gilbert, D. (2012). Hypoxia in the Lower St.
413 Lawrence Estuary: How physics controls spatial patterns. *Journal of Geophysical*
414 *Research*, 117(C7), C07018. <https://doi.org/10.1029/2011JC007751>

415 LeGrande, A. N., & Schmidt, G. A. (2006). Global gridded data set of the oxygen isotopic
416 composition in seawater. *Geophysical Research Letters*, 33(12).
417 <https://doi.org/10.1029/2006GL026011>

418 Levitus, S., Antonov, J. I., Baranova, O. K., Boyer, T. P., Coleman, C. L., Garcia, H. E., et al.
419 (2013). The World Ocean Database. *Data Science Journal*, 12(0), WDS229-WDS234.
420 <https://doi.org/10.2481/dsj.WDS-041>

421 Liu, W., Xie, S.-P., Liu, Z., & Zhu, J. (2017). Overlooked possibility of a collapsed Atlantic
422 Meridional Overturning Circulation in warming climate. *Science Advances*, 3(1).
423 Retrieved from <http://advances.sciencemag.org/content/3/1/e1601666.abstract>

424 Luo, H., Castelao, R. M., Rennermalm, A. K., Tedesco, M., Bracco, A., Yager, P. L., &
425 Mote, T. L. (2016). Oceanic transport of surface meltwater from the southern Greenland
426 ice sheet. *Nature Geoscience*, 9(7), 528–532. <https://doi.org/10.1038/ngeo2708>

427 Marcott, S. A., Clark, P. U., Padman, L., Klinkhammer, G. P., Springer, S. R., Liu, Z., et al.
428 (2011). Ice-shelf collapse from subsurface warming as a trigger for Heinrich events.
429 *Proceedings of the National Academy of Sciences of the United States of America*,
430 108(33), 13415–13419. <https://doi.org/10.1073/pnas.1104772108>

431 Moffa-Sánchez, P., Hall, I. R., Barker, S., Thornalley, D. J. R., & Yashayaev, I. (2014).
432 Surface changes in the eastern Labrador Sea around the onset of the Little Ice Age.
433 *Paleoceanography*, 29(3), 160–175. <https://doi.org/10.1002/2013PA002523>

434 Nusbaumer, J., Wong, T. E., Bardeen, C., & Noone, D. (2017). Evaluating hydrological
435 processes in the Community Atmosphere Model Version 5 (CAM5) using stable isotope
436 ratios of water. *Journal of Advances in Modeling Earth Systems*, 9(2), 949–977.
437 <https://doi.org/10.1002/2016MS000839>

438 Petrie, B., & Drinkwater, K. (1993). Temperature and salinity variability on the Scotian Shelf
439 and in the Gulf of Maine 1945–1990. *Journal of Geophysical Research*, 98(C11),
440 20079. <https://doi.org/10.1029/93JC02191>

441 Rahmstorf, S., Box, J. E., Feulner, G., Mann, M. E., Robinson, A., Rutherford, S., &
442 Schaffernicht, E. J. (2015). Exceptional twentieth-century slowdown in Atlantic Ocean
443 overturning circulation. *Nature Climate Change*, 5(5), 475–480.
444 <https://doi.org/10.1038/nclimate2554>

445 Saba, V. S., Griffies, S. M., Anderson, W. G., Winton, M., Alexander, M. A., Delworth, T.
446 L., et al. (2016). Enhanced warming of the Northwest Atlantic Ocean under climate
447 change. *Journal of Geophysical Research: Oceans*, 121(1), 118–132.
448 <https://doi.org/10.1002/2015JC011346>

449 Saenger, C., Came, R. E., Oppo, D. W., Keigwin, L. D., & Cohen, A. L. (2011). Regional
450 climate variability in the western subtropical North Atlantic during the past two
451 millennia. *Paleoceanography*, 26(2). <https://doi.org/10.1029/2010PA002038>

452 Sanchez-Cabeza, J. A., & Ruiz-Fernández, A. C. (2012). 210Pb sediment radiochronology:
453 An integrated formulation and classification of dating models. *Geochimica et*
454 *Cosmochimica Acta*, 82, 183–200. <https://doi.org/10.1016/j.gca.2010.12.024>

455 Schmittner, A., & Lund, D. C. (2015). Early deglacial Atlantic overturning decline and its
456 role in atmospheric CO₂ rise inferred from carbon isotopes (δ¹³C). *Climate of the Past*,
457 11(2), 135–152. <https://doi.org/10.5194/cp-11-135-2015>

458 Shackleton, N. J. (1974). Attainment of isotopic equilibrium between ocean water and the
459 benthonic foraminifera genus *Uvigerina*: Isotopic changes in the ocean during the last
460 glacial. *Colloques Internationaux Du C.N.R.S.*, 219, 203–210.

461 Sherwood, O. A., Lehmann, M. F., Schubert, C. J., Scott, D. B., & McCarthy, M. D. (2011).
462 Nutrient regime shift in the western North Atlantic indicated by compound-specific
463 δ¹⁵N of deep-sea gorgonian corals. *Proceedings of the National Academy of Sciences of*
464 *the United States of America*, 108(3), 1011–5. <https://doi.org/10.1073/pnas.1004904108>

465 St-Onge, G., Stoner, J. S., & Hillaire-Marcel, C. (2003). Holocene paleomagnetic records
466 from the St. Lawrence Estuary, eastern Canada: centennial- to millennial-scale
467 geomagnetic modulation of cosmogenic isotopes. *Earth and Planetary Science Letters*,
468 209(1–2), 113–130. [https://doi.org/10.1016/S0012-821X\(03\)00079-7](https://doi.org/10.1016/S0012-821X(03)00079-7)

469 Stouffer, R. J., Yin, J., Gregory, J. M., Dixon, K. W., Spelman, M. J., Hurlin, W., et al.
470 (2006). Investigating the Causes of the Response of the Thermohaline Circulation to
471 Past and Future Climate Changes. *Journal of Climate*, 19(8), 1365–1387.
472 <https://doi.org/10.1175/JCLI3689.1>

473 Thibodeau, B., de Vernal, A., & Mucci, A. (2006). Recent eutrophication and consequent
474 hypoxia in the bottom waters of the Lower St. Lawrence Estuary: Micropaleontological
475 and geochemical evidence. *Marine Geology*, 231(1–4), 37–50.
476 <https://doi.org/10.1016/j.margeo.2006.05.010>

477 Thibodeau, B., Lehmann, M. F., Kowarzyk, J., Mucci, A., Gélinas, Y., Gilbert, D., et al.
478 (2010b). Benthic nutrient fluxes along the Laurentian Channel: Impacts on the N budget
479 of the St. Lawrence marine system. *Estuarine, Coastal and Shelf Science*, 90(4), 195–
480 205. <https://doi.org/10.1016/j.ecss.2010.08.015>

481 Thibodeau, B., de Vernal, A., Hillaire-Marcel, C., & Mucci, A. (2010a). Twentieth century
482 warming in deep waters of the Gulf of St. Lawrence: A unique feature of the last
483 millennium. *Geophysical Research Letters*, 37(17).
484 <https://doi.org/10.1029/2010GL044771>

485 Thibodeau, B., de Vernal, A., & Limoges, A. (2013). Low oxygen events in the Laurentian
486 Channel during the Holocene. *Marine Geology*, 346, 183–191.
487 <https://doi.org/10.1016/j.margeo.2013.08.004>

488 Thornalley, D. J. R., Oppo, D. W., Ortega, P., Robson, J. I., Brierley, C. M., Davis, R., et al.
489 (2018). Anomalously weak Labrador Sea convection and Atlantic overturning during the
490 past 150 years. *Nature*, 556(7700), 227–230. <https://doi.org/10.1038/s41586-018-0007-4>

491 Wong, T. E., Nusbaumer, J., & Noone, D. C. (2017). Evaluation of modeled land-atmosphere
492 exchanges with a comprehensive water isotope fractionation scheme in version 4 of the
493 Community Land Model. *Journal of Advances in Modeling Earth Systems*, 9(2), 978–
494 1001. <https://doi.org/10.1002/2016MS000842>

495 Yang, Q., Dixon, T. H., Myers, P. G., Bonin, J., Chambers, D., & Van Den Broeke, M. R.
496 (2016). Recent increases in Arctic freshwater flux affects Labrador Sea convection and
497 Atlantic overturning circulation. *Nature Communications*, 7.
498 <https://doi.org/10.1038/ncomms10525>

499 Yashayaev, I., & Loder, J. W. (2016). Recurrent replenishment of Labrador Sea Water and
500 associated decadal-scale variability. *Journal Geophysical Research: Oceans*, *121*,
501 8095–8114. <https://doi.org/10.1002/2016JC012046>. Received
502 Yu, L., Gao, Y., & Otterå, O. H. (2016). The sensitivity of the Atlantic meridional
503 overturning circulation to enhanced freshwater discharge along the entire, eastern and
504 western coast of Greenland. *Climate Dynamics*, *46*(5–6), 1351–1369.
505 <https://doi.org/10.1007/s00382-015-2651-9>
506 Zhang, J., Liu, Z., Brady, E. C., Oppo, D. W., Clark, P. U., Jahn, A., et al. (2017).
507 Asynchronous warming and $\delta^{18}\text{O}$ evolution of deep Atlantic water masses during the
508 last deglaciation. *Proceedings of the National Academy of Sciences*, *114*(42), 11075–
509 11080. <https://doi.org/10.1073/pnas.1704512114>
510 Zhang, R. (2008). Coherent surface-subsurface fingerprint of the Atlantic meridional
511 overturning circulation. *Geophysical Research Letters*, *35*(20), L20705.
512 <https://doi.org/10.1029/2008GL035463>
513 Zhang, R., Vallis, G. K., Fluid, G., Oceanic, N., & Program, O. S. (2007). The Role of
514 Bottom Vortex Stretching on the Path of the North Atlantic Western Boundary Current
515 and on the Northern Recirculation Gyre. *Journal of Physical Oceanography*, *37*(8),
516 2053–2080. <https://doi.org/10.1175/JPO3102.1>
517 Zhu, J., Liu, Z., Brady, E. C., Otto-Bliesner, B. L., Marcott, S. A., Zhang, J., et al. (2017).
518 Investigating the Direct Meltwater Effect in Terrestrial Oxygen-Isotope Paleoclimate
519 Records Using an Isotope-Enabled Earth System Model. *Geophysical Research Letters*,
520 *44*, 12501–12510. <https://doi.org/10.1002/2017GL076253>
521 Zhu, J., Liu, Z., Brady, E., Otto-Bliesner, B., Zhang, J., Noone, D., et al. (2017). Reduced
522 ENSO variability at the LGM revealed by an isotope-enabled Earth system model.
523 *Geophysical Research Letters*, *44*(13), 6984–6992.
524 <https://doi.org/10.1002/2017GL073406>
525
526